CrystEngComm

View Online / Journal Homepage
Dynamic Article Links

Cite this: DOI: 10.1039/c1ce06096a

www.rsc.org/crystengcomm

HIGHLIGHT

Radicals organized by disk shaped aromatics – polymorphism and co-crystals that tune inter-electron exchange†

Handan Akpinar,[a] Joel T. Mague,[b] Miguel A. Novak,[cd] Jonathan R. Friedman[e] and Paul M. Lahti*[a]

DOI: 10.1039/c1ce06096a

Polymorphism's effect on intermolecular packing is a critical consideration for organic magnetic materials. Magnetostructural studies of pyrene-1-yl (Pyr) bearing nitronylnitroxide (NN) and iminoylnitroxide (IN) radicals found that PyrNN gives two allotropes: one has spin-paired dyads with $\Delta E = J/k \approx -178$ K, and one is half spin-paired with $\Delta E = J/k \approx -102$ K, and half paramagnetic. PyrIN also gives two allotropes, one an *anti* conformation that is spin paired with $\Delta E = J/k = -410$ K, and one a paramagnetic system having a *syn* conformation. PyrNN co-crystallizes with C_6F_6 in 2 : 1 ratio with a methyl to nitroxide contact network exhibiting low dimensional 1-D or 2-D antiferromagnetic exchange.

Introduction

The magnetism of purely organic, crystalline molecular materials has proven to be a subtle and complex area of materials science. Structure-property relationships between crystal packing of organic radicals and observed magnetic behaviour have been and remain particularly important,[1] especially because simplistic consideration only of closest contacts between sites of large spin density frequently are not predictive[2] of observed magnetic behaviour. Exchange interactions between unpaired spins as a function of fairly small changes in crystal packing provide many challenges for solid-state physical organic chemistry.

[a]Department of Chemistry, University of Massachusetts, Amherst, MA, 01003, USA. E-mail: lahti@chem.umass.edu; Tel: +1-413-545-2291
[b]Department of Chemistry, Tulane University, New Orleans, LA, 70118, USA. E-mail: joelt@tulane.edu
[c]Instituto de Física, Universidade Federal do Rio de Janeiro, Rio de Janeiro-RJ, 21945-970, Brazil. E-mail: mnovak@if.ufrj.br
[d]Visiting Scholar, University of Massachusetts, Amherst, MA, 01003, USA
[e]Department of Physics, Amherst College, Amherst, MA, 01002, USA. E-mail: jrfriedman@amherst.edu

† Electronic supplementary information (ESI) available: pictures of crystals, experimental procedures, magnetization *versus* field data for all samples, magnetic data plots with fitting equations and statistics, archival summaries of model computations of inter-radical exchange coupling and spin density computations for PyrNN, and both *anti*- and *syn*-PyrIN. Includes multiple files allowing manipulation of schemes and figures. CCDC reference numbers 840778–840782. For ESI and crystallographic data in CIF or other electronic format see DOI: 10.1039/c1ce06096a

Handan Akpinar

Handan Akpinar received her BS (2004) and MS (2006) in Chemistry from Middle East Technical University (Turkey). Currently, she is enrolled in the PhD graduate program in chemistry at University of Massachusetts Amherst (USA). Her graduate research focuses on molecular magnetism, organic radicals and crystal engineering.

Joel T. Mague

Joel T. Mague is Professor of Chemistry and Director of the Tulane University Crystallographic Laboratory. He has been at Tulane University since 1966 and has served a number of terms as Associate Chair and Chair of the Chemistry Department. His research interests include the synthesis and structure of network solids based on functionalized carboxylic acids and x-ray crystallography.

For this reason, polymorphism is always of potential concern when studying organic magnetic materials, but also provides an opportunity to modulate magnetic behaviour

In this article, we exemplify the possibilities of polymorphous behaviour by comparative magnetostructural investigations of 2-(1′-pyrenyl)-4,4,5,5-tetramethyl-4,5-dihydro-*1H*-imidazole-3-oxide-1-oxyl (PyrNN) and 2-(1′-pyrenyl)-4,4,5,5-tetramethyl-4,5-dihydro-*1H*-imidazole-1-oxyl (PyrIN). As part of our long-standing interest in the assembly of organic radicals, we tested their solid-state assembly and resultant magnetic behaviours under different crystallization conditions. The crystallography of these compounds is in great part determined by packing of their large, disk-shaped, rigid aromatic groups, since they have no substituent functionality that promotes directional assembly (*e.g.*, hydrogen bonding). Rigid, flat, disk-like aromatic groups tend to π-stack or form T-contacts in manners common to many benzenoid aromatic molecules.[3] However, such aryl-aryl interactions will not directly affect magnetic effects that will be dominated by close contact approaches between the small, localized radical units in PyrNN and PyrIN. Alteration of the intermolecular contact geometries between radical units was attempted by changing crystallization conditions, including addition of hexafluorobenzene (C_6F_6), which is known to co-crystallize with some hydrocarbon aromatics to give[4] alternating hydrocarbon and fluorocarbon aromatics (–H–F–H–F–) within a π -stack.

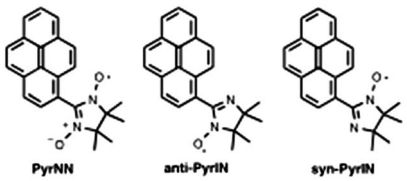

Polymorphic phase formation was found for both PyrNN and PyrIN, with corresponding differences in the magnetic behaviours of the phases. Also, PyrNN forms completely different intermolecular contacts and magnetic exchange interactions, depending on whether it is crystallized alone, or as a co-crystal with hexafluorobenzene.

Experimental methods

PyrNN and PyrIN were made‡ using typical literature synthetic procedures,[5] from pyrene-1-carboxaldehyde. Details are given in supporting material. Crystallization from acetonitrile gave PyrNN as small, very deep blue, shiny prisms with well-formed faces. From dichloromethane/acetonitrile it gave long, broad, thin plates or prisms that looked blue to blue-brown, depending on lighting and crystal thickness. PyrIN formed variably shaped crystals, depending on recrystallization conditions. Crystallization from ethyl acetate plus hexane yielded both large red-orange blocks (up to 10 mm largest dimension) and blades– single–crystal X-ray diffraction (XRD) analysis showed that both had the same space group and lattice parameters. But, slow evaporation under nitrogen of chloroform solutions of the original (block/blade) crystals layered below methylcyclohexane yielded clusters of deep red needles that look very different. Both

‡ **PyrIN**: Mp = 190–191 °C; EPR (toluene, 9.647 GHz): a_N = 7.18 gauss (2 N); MS (FAB) found *m/z* = 341.2, calculated for $C_{23}H_{21}N_2O_1$ *m/z* = 341.2. **PyrNN**: Mp = 150–151 °C; EPR (toluene, 9.647 GHz), a_N = 8.85, 4.00 gauss; MS (FAB) found *m/z* = 357.2, calculated for $C_{23}H_{21}N_2O_2$ *m/z* = 357.2. **$(PyrNN)_2 \cdot C_6F_6$**; Mp = 193–195 °C.

Miguel A. Novak

Miguel A. Novak is Professor of Physics at the Federal University of Rio de Janeiro and research fellow of Conselho Nacional de Desenvolvimento Científico e Tecnológico, Brazil. His research interests are in Condensed Matter Physics, focused in nanomagnetism and molecular magnetism, with fundamental contributions on organic magnetism, single molecule magnets and single chain magnets. His role in work that found resonances between high-spin states of single-molecule magnets was recognized in 2008 as a Nature Milestone in spin chemistry.

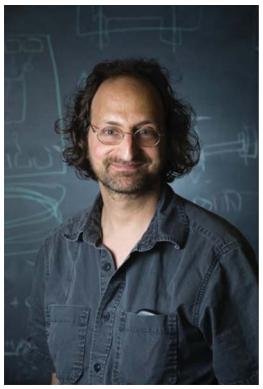

Jonathan R. Friedman

Jonathan R. Friedman is Associate Professor of Physics at Amherst College. He has been Chair of the Department since 2010. His research focuses on the magnetization dynamics of single-molecule magnets and the quantum properties of superconducting "qubits". He was the recipient of a prestigious NSF CAREER award. For his pioneering discovery of tunneling in single-molecule magnets, he shared the 2002 Europhysics Prize. In 2008, Nature Physics dubbed the discovery one of 23 "milestones" in the history of spin physics.

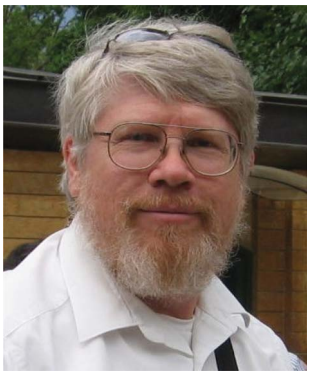

Paul M. Lahti

Paul M. Lahti is Professor of Chemistry (UMass Amherst since 1985) and co-Director of a U.S. DOE-funded Energy Frontier Research Center at the University of Massachusetts Amherst. He has served terms as department head and associate dean, and received outstanding teaching (1994), research (2007), and service (2009) awards. His research interests include photo-processes in organic-based photovoltaics and LEDs, molecule based magnetism, control of molecular crystallization, and spectroscopy of open-shell molecules.

Table 1 Crystallographic parameters for materials studied

	α-PyrNN	β-PyrNN	α-PyrIN	β-PyrIN	$(PyrNN)_2 \cdot C_6F_6$
T/K	100	100	100	293	100
Formula	$C_{23}H_{21}N_2O_2$	$C_{23}H_{21}N_2O_2$	$C_{23}H_{21}N_2O$	$C_{23}H_{21}N_2O$	$C_{26}H_{21}N_2O_2 \cdot 0.5(C_6F_6)$
Formula weight	357.4	357.4	343.0	343.0	450.45
Crystal system	Monoclinic	Monoclinic	Monoclinic	Monoclinic	Monoclinic
Space group	$P2_1/n$	$P2_1/n$	$P2_1/n$	$P2_1$	$P2_1/n$
a/Å	14.428(2)	9.856(2)	10.322(5)	7.6366(7)	15.380(2)
b/Å	7.4972(12)	7.2899(17)	7.181(3)	15.5557(14)	7.4688(11)
c/Å	33.289(5)	25.019(6)	24.037(11)	15.0141(14)	18.268(3)
α (°)	90.0	90.0	90.0	90.0	90.0
β (°)	91.483(2)	94.210(3)	98.018(6)	90.395(1)	97.9670(13)
γ (°)	90.0	90.0	90.0	90.0	90.0
V/Å^3	3556.4(9)	1792.7(7)	1764.3(14)	1783.5(3)	2075.6(5)
Formula *Z*	8	4	4	4	4
D_c/Mg m^{-3}	1.34	1.32	1.285	1.27	1.44
μ/mm^{-1}	0.086	0.085	0.080	0.078	0.110
F(000)	1512	756	724	724	936
R_1 ($N > 2\sigma$)	0.0723 (3478)	0.0417 (4115)	0.0399 (3197)	0.0989 (6382)	0.0439 (4547)
wR_2 (all)	0.1407 (7335)	0.1171 (4652)	0.1143 (4021)	0.2891 (8133)	0.1204 (5299)
GOF (*S*)	0.96	1.04	1.03	1.05	1.03
$\Delta\rho_{max}$, $\Delta\rho_{min}$ (e-Å^{-3})	0.23, −0.27	0.40, −0.27	0.25, −0.19	0.54, −0.41	0.44, −0.29
CCDC Deposition No.	840779	840780	840782	840778	840781

PyrNN and PyrIN were also subjected to simple, evaporative crystallization from C_6F_6; PyrIN did not give diffraction quality crystals, but PyrNN did yield a co-crystalline material. Crystallographic and structure refinement parameters for these are given in Table 1. Specific procedures for crystallographic studies, pictures of example crystals, and electronic files of crystal packing are given in ESI.†

Magnetic measurements were obtained using Quantum Design MPMS-7 (UMass) or PPMS-9 (Amherst) magnetometers. Crushed polycrystalline samples were placed in a gelatin capsule and held in place with a wad of cotton. The capsule was placed in a plastic straw and then put into the magnetometer sample rod for insertion. The magnetic behaviour was measured over 1.8–300 K at fixed external fields as described below; magnetization *versus* field data were obtained at 1.8 K. Throughout this paper, for fittings of susceptibility data *vs.* temperature, exchange constants will be given using the spin Hamiltonian $H = -JS_1 \cdot S_2$, ($J/k < 0$ for antiferromagnetic = AFM exchange) unless otherwise stated.

Results and discussion

The crystal structure of PyrNN has been reported as a private communication to the Cambridge Structural Databank (CSD).[6] PyrNN was also mentioned as a synthetic intermediate[7] in a study of PyrIN by Zhang, Zhu, and coworkers, where PyrIN was tested as a possible "AND" logic gate molecule, based upon changes to its fluorescence behaviour. Zhang, Zhu, and coworkers later studied PyrIN as a component in solid-state field effect transistor (FET) devices.[8] A crystal structure for PyrIN was reported in the latter work, as well as a linear Curie–Weiss plot of $1/\chi$ *vs.* *T* with a slope that indicated essentially pure $S = ½$ spin carriers. The data yielded a Weiss constant of $\theta = -0.78$ K, indicating weak antiferromagnetic (AFM) exchange interactions.

PyrNN polymorphs and magnetic behaviour

The first crystal structure we obtained for PyrNN was essentially the same as that given by Mann *et al.*[6] in their private communication. Hereafter, this will be described as α-PyrNN. There are two crystallographically distinct molecules differing in the amount of torsion about the bond linking the NN unit to the pyrene ring. Fig. 1 shows ORTEP representations of the distinct molecules, while Fig. 2 shows the crystal packing in the structure, labeling the distinct molecules as Forms 1 and 2. Both have N–O to nitronylnitroxide methyl group close contacts; because the methyl groups have small spin densities, these could affect exchange. Form 2 has numerous N–O to pyrene HC contacts that assist molecular assembly, but these should not affect exchange due to the lack of spin density on the pyrene unit.

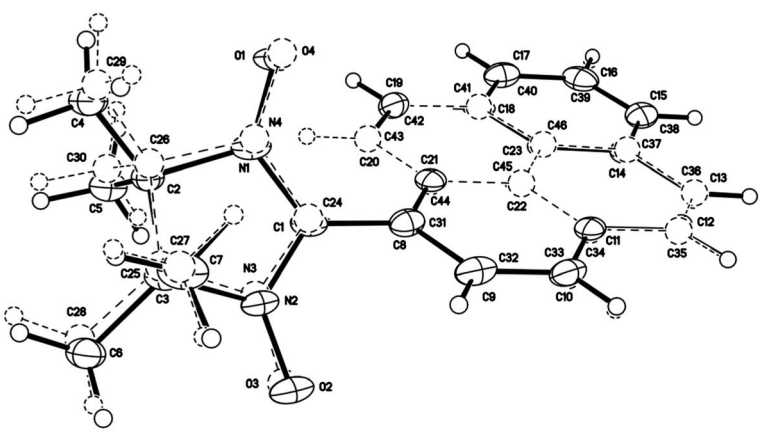

Fig. 1 ORTEP structure overlay of two distinguishable molecules in α-PyrNN at 100 K. Thermal ellipsoids are shown at 50% probability.

Viewed down the crystallographic *b*-axis (Fig. 2), the two forms segregate into alternating, sheet-like regions that parallel the *ab*-plane. Form 1 stacks along the *b*-axis; the stacks are related by the two-fold screw axes along the *a*-axis. The pyrene rings are slip-stacked, but canted strongly so they have no π-orbital overlap, despite a pyrene-pyrene plane-to-plane distance of only 2.89 Å. The Form 1 stacks also form contacts along the *b*-axis from nitronylnitroxide methyl groups to neighbouring chain pyrene π-clouds at a distance of r[C6···C21′] = 3.365(4) Å. Form 2 molecules also form strongly canted slip-stacks along the *b*-axis (pyrene-to-pyrene plane-to-plane distance of 2.64 Å). The Form 2 stacks form interchain herringbone T-contacts of pyrene C–H bonds into the pyrene π-clouds of neighbouring Form 2 chains. They also form contacts between radical N–O groups on one stack to neighbouring pyrene C–H groups on another, with the other N–O group forming contacts to neighbouring radical methyl C–H groups on the other side. Finally, Form 1 and 2 stacks associate with one another through contacts between Form 1 N–O groups to Form 2 methyl groups, a N1–O1···H–C29(methyl) contact. Fig. 2 and Scheme 1 describe some of these contacts, and Table 2 gives some of the molecular and intermolecular parameters; additional information is given in the ESI.

Most notably from a spin assembly point of view, Form 1 has dyad pairwise contacts between nitronylnitroxide N–O groups related by inversion symmetry (Scheme 1); r[O2···N2′] = 3.291(4) Å and r[O2···O2′] = 3.348(3) Å in the structure at 100 K. The structure from Mann *et al.*[6] at 295 K has r[O2···O2′] = 3.445 Å. This contact gives good N–O···O–N SOMO–SOMO overlap, which should induce antiferromagnetic exchange. There are no analogously short contacts between N–O spin units in the Form 2 molecules, although the N1–O1 units of Form 1 have fairly close contacts with O3–N in form 2; r[O1···O3′] = 3.89 Å in Scheme 1. But, the "edge on" geometry of the O1···O3′ contact does not allow good SOMO–SOMO overlap, so it is expected *not* to give a strong exchange interaction. While the N–O to methyl group contacts can contribute to exchange interactions between spin units, these will be much smaller[2e] than the exchange that is due to the direct N–O···O–N spin orbital overlap, so it can be ignored as a major source of exchange here.

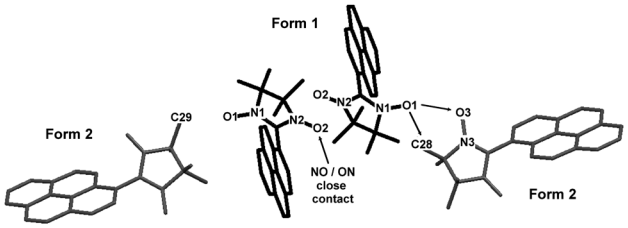

Scheme 1 Intermolecular contacts between radical sites in α-PyrNN.§

Fig. 3 shows magnetic susceptibility *versus* temperature data measured for α-PyrNN at 1000 Oe as a Curie–Weiss plot of 1/χ *versus T*, and as a χ*T vs. T* plot. The Curie–Weiss plot shows a change in slope in the 30–50 K temperature range. A linear fit to the data above 150 K gives a Curie constant of $C = 0.395 \pm 0.012$ emu K/Oe mol^{-1}, consistent with the value for $S = ½$ radical units; the abscissa intercept yields a Weiss constant of $\theta = -18.7 \pm 7.9$ K, indicating fairly strong AFM interactions. The uncertainties here and subsequently are 95% confidence limits. The 1/χ *versus T* data below 30 K yield $C = 0.203 \pm 0.003$ emu K/Oe mol^{-1} and $\theta = -0.6 \pm 0.2$ K. These results show spin pairing of half of the $S = ½$ spin carriers at low temperature with a lack of significant interspin exchange in the remaining spins.

The crystallography of α-PyrNN is expected to yield spin pairing of the Form 1 molecules across the O2···O2′ contact, with limited if any exchange among the Form 2 molecules due to lack of contacts with good inter-radical SOMO–SOMO overlap. A modified Bleaney–Bowers equation[9] including a paramagnetic contribution was used to fit the χ*T vs. T* data (eqn (1))

$$\chi T = \left[C \cdot \frac{2}{3 + \exp(-J_{ST}/kT)} \right] \cdot (1 - F) + (F) \cdot 0.375 \cdot \frac{T}{T - \theta}, \quad C = \frac{Ng^2\beta^2}{k} = 0.375 g^2 \qquad (1)$$

where the spin pairing energy from singlet to triplet is $\Delta E(\mathrm{S–T}) = -J_{ST}/k$, the fraction of paramagnetic molecules (Form 2) is *F*, and a generalized mean field correction θ can be included for the paramagnetic component. If $g = 2.007$ is fixed from EPR solution measurements of PyrNN, and no mean field term is used, and *F* is fitted, $J/k = -88 \pm 3$ K and $F = 0.485 \pm 0.006$. If the mean field term is included, and the g-value is fitted, with $F = 0.5$ fixed, a better fit is found with $g = 2.085 \pm 0.008$, $J/k = -102 \pm 2$ K and $\theta = -0.17 \pm 0.02$ K; this fit is shown in

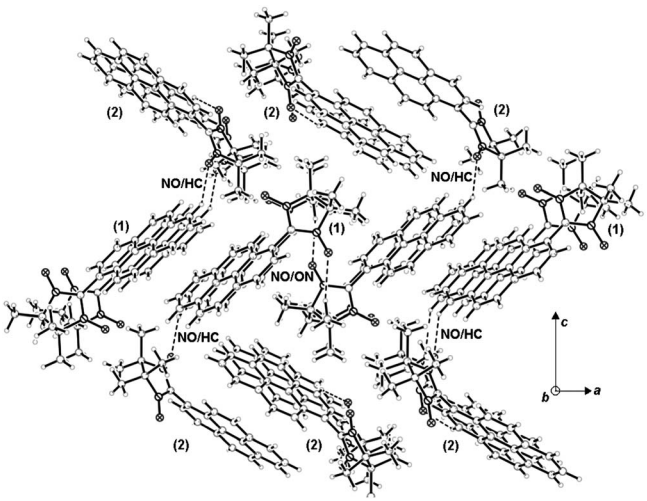

Fig. 2 Solid-state packing for α-PyrNN, showing regions of crystallographically distinct molecules, Forms (1) and (2); N–O···O–N and N–O···H–N close contacts are indicated.

Table 2 Inter-ring dihedral and selected intermolecular contact parameters for α-PyrNN, β-PyrNN, α-PyrIN, β-PyrIN, $(PyrNN)_2 \cdot C_6F_6$[a]

	Torsion[a]	Antiparallel[b] NO···ON	Antiparallel[b] NO···N	NO···C
α-PyrNN	−47.16° ∠C9–C8–C1–N2 [*f1*] −49.96° ∠C32–C31–C24–N3 [*f2*]	3.348 Å (O2[*f1*]···O2′[*f1*]) 3.886 Å (O1[*f1*]···O3′[*f2*])	3.291 Å (O2···N2′)	3.955 Å (O1[*f1*]···C28′[f2])[c] 3.568 Å (O1[*f1*]···C29′[f2])[c] 3.509 Å (O2[*f1*]···C5′[*f1*])[cd] 3.302 Å (O3[*f2*]···C30″[*f2*])[c] 3.302 Å (O4[*f2*]···C27′[*f2*])[c]
β-PyrNN	−46.44° ∠C9–C8–C1–N2	*3.367 Å (O2···O2′, 293 K)* 3.291 Å (O2···O2′, 100 K) 4.241 Å (O2···O2′, 100 K)	*3.333 Å (O2···N2′, 293 K)* 3.237 Å (O2···N2′, 100 K)	3.371 Å (O1···C5′, 100 K)[cd] 3.592 Å (O1···C6′, 100 K)[cd]
α-PyrIN	+43.55° ∠C9–C8–C7–N1	*3.302* Å (O1···O1′, 293 K)[e] 3.157 Å (O1···O1′, 100 K)	*3.254* Å (O1···N1′, 293 K)[e] 3.068 Å (O1···N1′, 100 K)	3.449 Å (O3···C5′, 100 K)[c] 3.975 Å (O3···C3′, 100 K)[c]
β-PyrIN [293 K]	*+56.12° ∠C9–C8–C1–N1 [f1]* *+52.68° ∠C32–C31–C24–N4 [f2]*	*none*	*none*	*(1–2 N–O···C(aryl) contacts for each PyrIN of the lattice, all <4 Å)*
$(PyrNN)_2 \cdot C_6F_6$	−47.22° C9–C8–C1–N2	none	none	3.315 Å (O2···C4′, 100 K)[c] 3.267 Å (O1···C6′, 100 K)[c] 3.525 Å (O2···C7′, 100 K)[c]

f1 = form 1, *f2* = form 2. Most values at 100 K, room temperature values in *italics*.[a] All torsions relative to the anti-PyrIN conformer as 0°. Positive torsions given anticlockwise looking down the interannular bond with pyrene in back, and the radical in front, relative to the C–N bond that is anti to the centroid of the pyrene; negative torsions have a clockwise twist using the same definition. [b] Closest intermolecular contacts between radical N–O groups, up to 5 Å. [c] Closest intermolecular N–O···C(methyl) contacts. [d] Involves NO···C contact associated with a close contact NO···ON dyad. [e] From ref. 8.

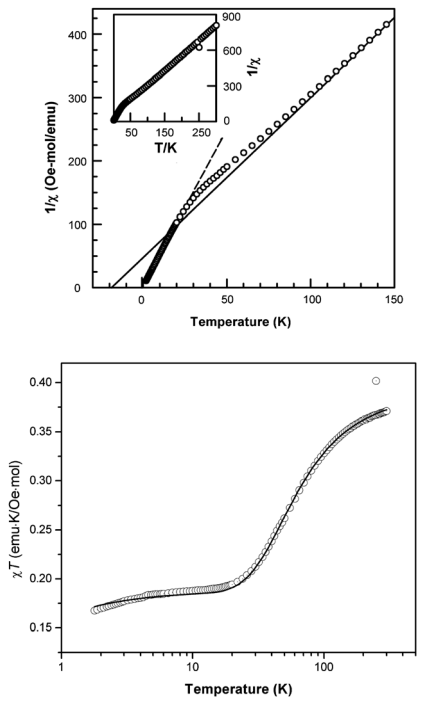

Fig. 3 Magnetic measurements for α-PyrNN in dc external field of 1000 Oe. Upper chart shows $1/\chi$ *vs.* *T* plot from 1.8–150 K (inset shows full temperature range of 1.8–300 K); solid line shows linear fit to data above 150 K, dashed line shows fit to data below 30 K. Lower chart shows χT *vs.* *T* data from 1.8–300 K; solid line shows fit to the half-dimer model described in the text, with fixed 50% of spins paired and a fitted mean field term θ.

Fig. 3. The small downturn in the χT *vs.* *T* data below 10 K (fitted by the mean field term) may be due to small AFM interactions between Form 2 molecules. Because the Form 1 molecules are strongly spin paired at 1.8 K, they make no contribution to low temperature saturation magnetization, which is about half the value of 5585 emu/mol expected for a mole of $S = ½$ spin units (see ESI). Overall, the magnetic behaviour of α-PyrNN is consistent with expectations based on its crystallography.

As described above, a new polymorph of PyrNN was found in this study, hereafter called β-PyrNN. Fig. 4 shows an ORTEP diagram, and Fig. 5 shows its solid-state packing. The new polymorph is crystallographically more orderly than the α-allotrope, with only one form of the molecule. All nitronylnitroxide groups form close-contact N2–O2···O2′–N2 dyads conducive to good SOMO–SOMO overlap, similar to those of Form 1 in α-PyrNN. The O2···O2′ distance is almost 0.08 Å longer at room temperature than at 100 K. There are also longer, secondary N–O···O–N contacts associated with the close-contact dyads, at an O2···O2″ distance of 4.24 Å; in effect, this gives an alternating chain of N2–O2···O2–N2 contacts as shown in Scheme 2. The N1–O1 group does *not* form close contacts with methyl groups, unlike the analogous situation in α-PyrNN, (compare Fig. 2 and 5). Instead, it forms herringbone T-contacts (C–H to π interactions) with pyrene units. These are not magnetically relevant due to the lack of spin density on the pyrene units, so they are only shown in Fig. 5.

Table 2 compares molecular inter-ring torsion angles found in the various solid phases, as well as selected intermolecular contact parameters involving radical sites

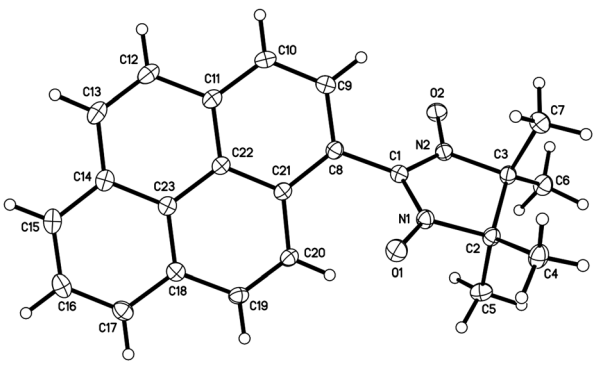

Fig. 4 ORTEP diagram for β-PyrNN at 100 K. Thermal ellipsoids are shown at 50% probability.

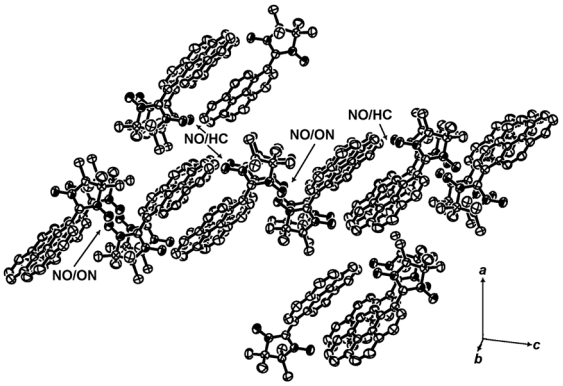

Fig. 5 Solid-state packing for β-PyrNN. N–O···O–N and N–O···H–C(aryl) close contacts are indicated.

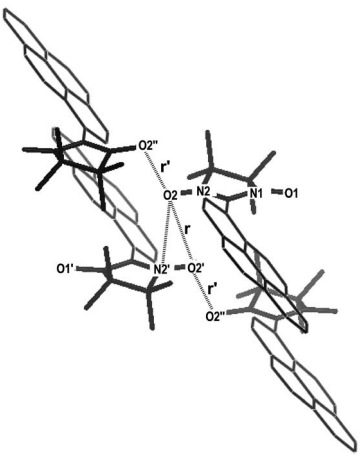

Scheme 2 Alternating intermolecular contacts in β-PyrNN. Distance r is the closest intra-dyad contact between radicals; distance r' is the longer, inter-dyad inter-radical contact. §

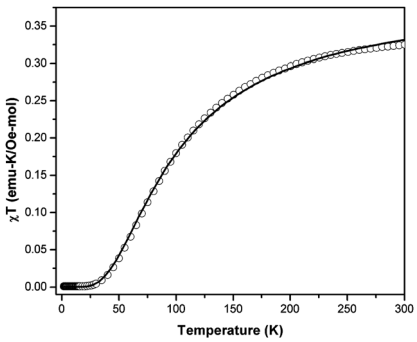

Fig. 6 Magnetic measurements for β-PyrNN in dc external field of 1000 Oe; χT *vs.* T data from 1.8–300 K; solid line shows fit to the spin pairing model of eqn (1), without mean field term, but including a paramagnetic fraction F.

with significant spin density. Overall, β-PyrNN should favor fairly strong spin pairing of all radical units, rather than only half as in α-PyrNN.

Fig. 6 shows the χT *vs.* T data for β-PyrNN obtained at 1000 Oe. The data do show the expected spin pairing behaviour. The data were fitted to the eqn (1) model, without inclusion of any mean field terms, to yield $g = 2.061 \pm 0.004$, $J/k = -178 \pm 2$ K and $F = 0.0008 \pm 0.002$. The very small paramagnetic impurity term is consistent with magnetization *versus* field measurements at 1.8 K, which show virtually no magnetic moment; at this temperature, all of the spins of β-PyrNN are strongly paired. The larger spin pairing energy for the β-form *versus* the α-form presumably reflects a better SOMO–SOMO overlap geometry, since small offset differences in the antiparallel arrangement between the N–O can significantly influence exchange.

The spin-pairing exchange energies of the Form 1 dyads of α-PyrNN and the dyads of β-PyrNN were estimated computationally using Gaussian[10] using the room temperature crystal structure contacts for the nitronylnitroxide moieties *only* (pyrene replaced by hydrogen). Both UB3LYP[11]/6-31G* and UB97D/6-31+G(d) computations were carried out; the latter uses Grimme's dispersion-corrected[12] functional. For both types of calculation, the $S = 0$ state was modeled[13] using a broken symmetry, unrestricted wavefunction. The singlet to triplet energy gap was corrected for effects of spin contamination in the broken symmetry $S = 0$ result by Yamaguchi's[14] method.

For α-PyrNN, at the UB3LYP/6-31G* level the computed ΔE(S–T) = 23.5 K; at the UB97D/6-31+G(d) level ΔE(S–T) = 63.7 K; here, ΔE(S–T) > 0 means a low spin ground state. For β-PyrNN, at the UB3LYP/6-31G* level the computed ΔE (S–T) = 76 K; at the UB97D/6-31+G(d) level ΔE(S–T) = 117 K. These results are in reasonable accord with the experimental results for magnetism, especially given that the AFM exchange will likely grow stronger as the crystal lattice contracts at low temperatures.

PyrIN polymorphs and magnetic behaviour

The crystal structure reported by Zhang and Zhu for PyrIN shows[5] close contacts between iminoylnitroxide N–O spin units, related by inversion symmetry and roughly antiparallel in a manner analogous to the situation in PyrNN. We obtained a very similar structure.¶ Fig. 7 shows an ORTEP representation of the structure from the present study, and Fig. 8 shows a packing diagram with the close contacts between N–O groups. At room temperature we found PyrIN to have virtually the same intermolecular packing distances found by Zhang and Zhu. The PyrIN molecules form dyads with close (N)O1···O1′(N) contacts, with r[O1···N1′] = 3.254(2) Å with r[O1···O(1) a′] = 3.302(2) Å. At 100 K the unit cell volume is decreased by 2.2% relative to that reported[5] at room temperature. More notably, at 100 K r[O1···N(1)′] = 3.068(2) Å and r[O1···O1′] = 3.157(2) Å, strong decreases compared to the room temperature distances. The dyads are also associated pairwise by methyl to pyrene π-cloud contacts (Scheme 3) with r[C6···C14′] = 3.478(3) Å, which again assist molecular assembly, but do not involve significant spin density sites and so are not expected to provide intermolecular exchange pathways.

Based on this structure, *stronger* AFM spin pairing should occur in PyrIN than in PyrNN, since the PyrIN geometry gives almost perfectly aligned SOMO–SOMO

§ A user-manipulatable Mercury[21] (.mryx) format file available for this scheme or figure in ESI.

¶ α-PyrIN has minor conformer disorder or remnant PyrNN based on our O-atom position occupancies in different models. Also, see ref. 8 vis-à-vis T. Yama, T. Hidekuma and Y. Teki, *Prepr. Symp. Ann. Mtg. Jpn. Soc. Molec. Sci.*, 2011, abstract 2P037.

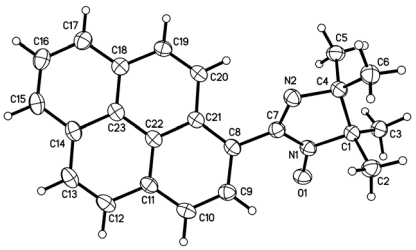

Fig. 7 ORTEP diagram for α-PyrIN at 100 K. Thermal ellipsoids are shown at 50% probability.

overlap with N1–O1 groups antiparallel at an even *closer* approach distance. Thus, we were initially surprised to find isolated spin, paramagnetic behaviour for samples of PyrIN, similar to that reported[5] by Zhang and Zhu. The difference in physical appearance of samples from different crystallizations of PyrIN led us to suspect that the paramagnetic behaviour was associated with an allotrope having different packing. The allotrope whose crystal structure was first reported[5] by Zhang and Zhu will be designated α-PyrIN in this article. By trying different crystallization conditions, another allotrope was found, β-PyrIN, with a different molecular conformer and quite different crystal packing.

Whereas α-PyrIN forms dark red needles in clumps, β-PyrIN forms cube-like blocks up to 1 mm on an edge, often simultaneously with large, red transparent blades. There are two crystallographically independent molecules of PyrIN (Fig. 9) in this phase, both of which are subject to "whole-molecule" disorder. This occurs by the pyrene portions occupying highly overlapping and nearly equally populated sites for each molecule, with the pyrene unit in one component "flipped over" relative to that in the other unit. The iminoylnitroxide unit positions are also disordered but significantly overlapped. Fig. 10 shows the lattice and the disorder in the two independent molecule sites. Both α-PyrIN and β-PyrIN are monoclinic, but their otherwise very different packing derives from a simple conformational difference. All β-form PyrIN molecules have a *syn* conformation with the iminoylnitroxide N–O group folded close to the pyrene unit. In the α-form the N–O group points *away* from pyrene, an *anti*-type conformation. Despite all the intermolecular contact variations in β-PyrIN in its disordered sites, it has no N–O···O–N contact closer than 7 Å. At distances >4.5 Å, exchange between nitronylnitroxide units becomes negligible, so, the β-PyrIN allotrope should not exhibit significant interspin exchange.

The magnetic behaviours of α-PyrIN and β-PyrIN in a dc field of 1000 Oe are compared in Fig. 11 as χT *vs.* T plots. The β-form exhibits the behaviour expected from its crystal structure: it is an $S = ½$ Curie paramagnet with essentially no intermolecular interactions. The α-form, by contrast, does not even show a higher

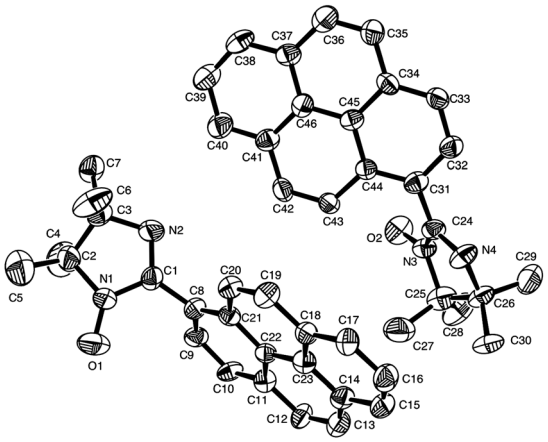

Fig. 9 ORTEP diagram for β-PyrIN molecules at room temperature; alternate, disordered positions not shown. Thermal ellipsoids are shown at 50% probability.

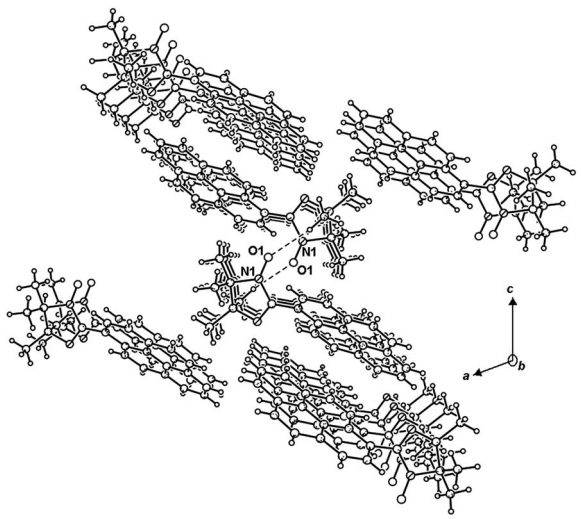

Fig. 8 Solid-state packing diagram for α-PyrIN at 100 K, showing the N–O···O–N close contacts.

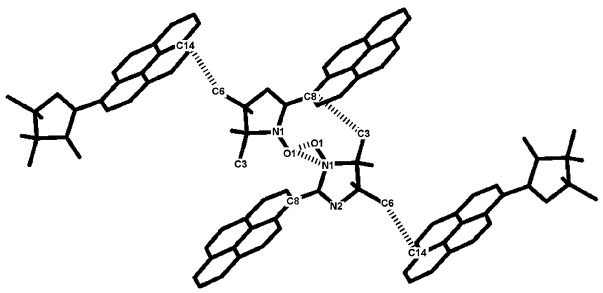

Scheme 3 Close intermolecular contacts in α-PyrIN.§

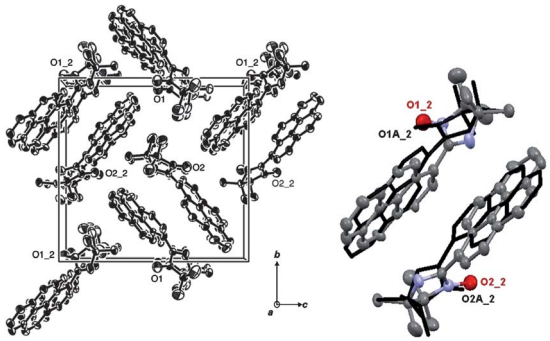

Fig. 10 Solid-state packing diagram for β-PyrIN (left, only one variant at a disordered site is shown): ORTEP diagrams§ with whole-molecule disorder (right). Thermal ellipsoids are shown at 50% probability.

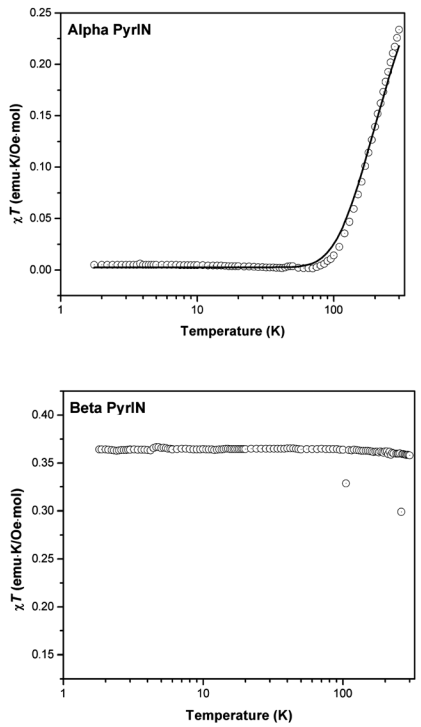

Fig. 11 Magnetic χT *vs.* T data for α-PyrIN (above) and β-PyrIN (below) in dc external field of 1000 Oe, both for 1.8–300 K. The upper chart, the solid line shows the fit to eqn (1) with no mean field term and inclusion of paramagnetic spin fraction F.

temperature plateau. Instead, χT at room temperature is already well below the expected value of 0.375 emu K/Oe mol^{-1}, and drops rapidly nearly to zero by 80 K. This is consistent with the strong AFM spin pairing exchange expected from the close N–O contacts in the α-form. Fitting of the data to eqn (1), with no mean field term, assuming $g = 2.007$, and allowing the paramagnetic term F to vary, gives a good fit for $J/k = -414 \pm 6$ K with $F = 0.7 \pm 0.4\%$. The small paramagnetic component likely arises from a small number of disordered, *syn*-conformer molecules in the lattice dominated by spin-paired *anti*-conformer molecules. Computation of the expected singlet to triplet splitting for α-PyrIN, using the same methodology used for PyrNN at the 100 K geometry for the close N–O contact between iminoylnitroxide groups (with the pyrene units replaced by hydrogen), gives ΔE(S–T) $= -J/k = 362$ K, at the UB3LYP/6-31G* level, and ΔE(S–T) $=$ 545 K at the UB97D/6-31+G(d) level. These computed results are in reasonable accord with the strong spin pairing in α-PyrIN. They are stronger than the PyrNN exchange couplings, in part, because more spin density is concentrated in the N–O units of PyrIN.

Crystallization of PyrIN and PyrNN from C_6F_6

Co-crystallization of PyrNN and PyrIN from C_6F_6 was attempted in an effort to "tune" their intermolecular contacts and exchange. Salmon-coloured needle-like crystals were obtained using PyrIN, with visible defects and void spaces. These "needles" did not diffract well, suggesting that any co-crystal lattice collapsed with loss of C_6F_6 upon standing. Dissolving these needles in toluene gave blood red solutions showing the EPR spectral 1 : 1 : 2 : 1 : 2 : 1 : 1 hyperfine septet pattern typically seen for PyrIN. Nominally equimolar concentrations of β-PyrIN compared to the "needles" of PyrIN obtained from C_6F_6 showed virtually identical spin counts. However, the salmon-coloured material showed only purely paramagnetic behaviour in a χT *vs.* T plot at 1000 Oe, with a Curie constant of C = 0.086 emu K/Oe mol^{-1} (see ESI). This corresponds to only 23% of the expected spins. Essentially the same solid-state spin yield was seen in the saturation magnetization of the sample at 1.8 K. Since the solution spin count shows all of the expected radical spins to be present in the defective crystals, but the solid magnetism shows only some of those spins, the remaining 77% of the radicals must be very strongly spin paired. Given the tendency of PyrNN and α–PyrIN to give spin pairing in the solid state, this scenario is plausible. Without a crystal structure, we do not know what geometry yields such strong AFM spin pairing. One can reasonably speculate that there must be very close contact and strong spin orbital overlap between large spin density sites of the iminoylnitroxide unit in some form of dyad arrangement.

By contrast to PyrIN, PyrNN from C_6F_6 gave readily flaked, blue plates that were visually different from the shiny, deep blue prisms of pure PyrNN. Increased sample weight relative to the input PyrNN, showed both PyrNN and C_6F_6 to be present. Crystallographic analysis showed the solid to be $(PyrNN)_2 \cdot C_6F_6$, whose molecular units are shown in Fig.12.

The 2 : 1 PyrNN : C_6F_6 stoichiometry is induced by two molecules of PyrNN "sandwiching" a C_6F_6 to give arene : fluoroarene : arene π-stacked triads. This follows the tendency[4] of fluorinated aromatics to form alternating π-stacks with hydrocarbon aromatics. The PyrNN·C_6F_6·PyrNN triads also form π–H–C T-type herringbone interactions with other triads, as shown in Fig. 13. But, looking down the *b*-axis, $(PyrNN)_2 \cdot C_6F_6$ packs into channels of high spin density nitronylnitroxide units linked by N–O···H–C(methyl) contacts, channels of pyrene units linked by π–H–C contacts, and channels of C_6F_6.These are viewed in Fig. 14 looking down the channels.

The inter-radical contacts in $(PyrNN)_2 \cdot C_6F_6$ are greatly changed by comparison to pure PyrNN. There are no direct close contacts between sites with large spin density. Instead of close contact dyads between radical N–O groups, chains of N–O···H–C(methyl) hydrogen bond type contacts form (Scheme 4); r(C4···O2′) = 3.3155(17) Å. Chains are further related to one another by two sets of similar but

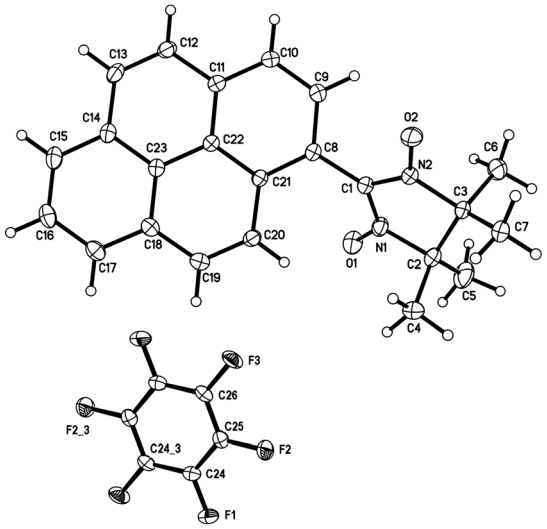

Fig. 12 ORTEP diagrams for symmetry distinct molecules in $(PyrNN)_2 \cdot C_6F_6$ at 100 K. Thermal ellipsoids are shown at 50% probability.

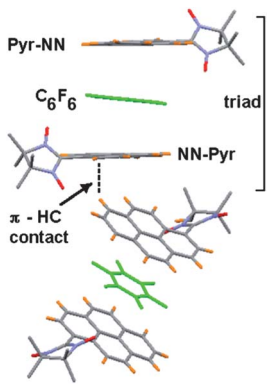

Fig. 13 A pair of $PyrNN \cdot C_6F_6 \cdot PyrNN$ triads, showing arene : fluoroarene : arene alternating π-stacking and π–cloud to H–C contacts between triads.§

distinct N–O···H–C contacts, shown in Fig. 14; rung A contacts r(C6···O1′) = 3.2665(19) Å and rung B contacts r(C7···O2′) = 3.5253(17) Å. Scheme 4 shows a side view of how two rails are linked by rung B contacts. The scheme also shows views of interchain hydrogen bonds of $C_6F_6$with both pyrene C–H bonds (F1···C12′, left view of scheme) and nitronylnitroxide methyl groups (F2···C5′, right view of scheme). Combining the views of Fig. 14 and Scheme 4, all of the N–O···H–C contacts can be considered to form corrugated 2-D sheets. Fig. 14 is coloured to emphasize this.

PyrNN in the co-crystal can be considered as being "shepherded" by the C_6F_6 molecules into forming the contacts shown in Fig. 13–14 and in Scheme 4.

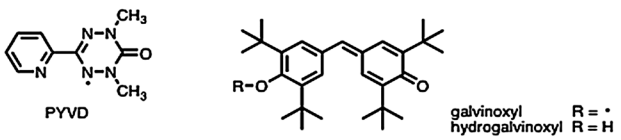

The C_6F_6 induces a more extended contact motif(chains, sheets) than occurs in PyrNN alone (dyads). Hicks and coworkers reported a comparable case, in which 1,5-dimethyl-3-(2-pyridyl)-6-oxoverdazyl, PYVD, is "shepherded" (our terminology) by hydroquinone into a well-organized, head-over-tail, π-stacked array with fairly strong 1-D AFM exchange interaction of J/k = −83 K. PYVD is not even persistent in the solid state for extended periods without hydroquinone co-crystallization.[15] Also, the exchange behaviour of galvinoxyl is strongly influenced by added diamagnetic hydrogalvinoxyl, which channels the radical component into a FM coupled packing arrangement that resists temperature-induced phase changes much more than pure galvinoxyl.[16]

The magnetic behaviour of the $(PyrNN)_2 \cdot C_6F_6$ co-crystal is shown in Fig. 15 as a χT *vs.* T plot. AFM exchange is still shown by the downturn in this plot, but weaker than in pure PyrNN. The data do not fit well to a spin pairing model, consistent with the lack of close N–O pairing. But, a Heisenberg 1-D AFM chain[17]model (Scheme 5) gives a very good fit with g = 1.999 and J_{1D}/k = −1.716 ± 0.003 K. A Heisenberg 2-D square planar AFM exchange model[18] also gave a good fit, with g = 2.0037 and J_{2D}/k = −0.986 ± 0.004 K. Details of the fitting equations are given in ESI. It is not straight forward to give preference to either the 1-D or 2-D exchange models from the crystallography in $(PyrNN)_2 \cdot C_6F_6$, since both are simplifications compared to the complex 2-D network of N–O···H–C(methyl) contacts. For example, the rail contacts in Scheme 4 seem appropriate for chain-like exchange, but the sequence of rung A and rung B contacts in Fig. 14 (lower view) could give similar behaviour; contributions from both could contribute to the results from the simplified square planar 2-D model. So, the co-crystal is probably best described as exhibiting fairly weak, low dimensional AFM exchange.‖

Gaussian[10] EPR-II level computations using a crystallographic geometry of PyrNN shows 0.04–1.6% spin densities on radical methyl groups; the spin densities on the pyrene unit atoms are even smaller, and can be considered negligible. Since the co-crystal lacks close contacts between N–O units, the modest experimental exchange constants are reasonable. Computational modeling of radical-site-only dyads for rail and rung contacts of Scheme 4, using the same procedure described earlier (replace pyrene by hydrogen atoms), gives ΔE_{rail}(S–T) = $-J_{rail}/k$ = −0.09 K, ΔE_{rungA}(S–T) = $-J_{rungA}/k$ = 0.75 K, and ΔE_{rungB}(S–T) = $-J_{rungB}/k$ = 0.85 K at the UB3LYP/6-31G* level, respectively. At the UB97D/6-31+G(d) level, the corresponding gaps are ΔE_{rail}(S–T) = −0.09 K, ΔE_{rungA}(S–T) = 0.95 K, and ΔE_{rungB}(S–T) = 2.20 K. Here, a positive number

‖ A spin ladder[22] is a tempting simplified magnetic model for the co-crystal, given the intermolecular contacts shown in Scheme 4. But, statistical analysis from such a fit shows over-parameterization, with high co-dependence of rail and rung exchange constants. So, no effort was made to use other models with multiple exchange constants. See the ESI for details.

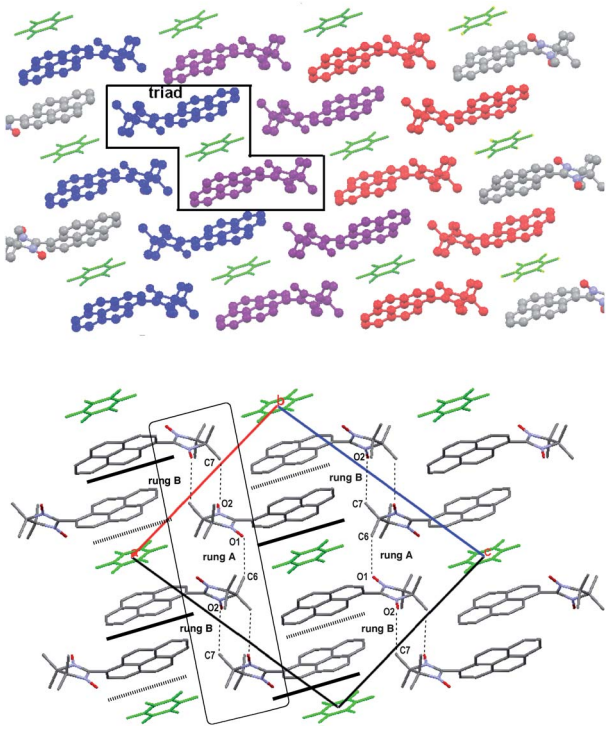

Fig. 14 Solid-state packing in co-crystalline $(PyrNN)_2 \cdot C_6F_6$, showing the *ac*-plane. Top view colour codes 2-D sheets of rungs (Scheme 4) associated by rung A and rung B contacts, with C_6F_6 in green. The lower view box labels N–O···H–C(methyl) rung A C6–(H)···O1′ and rung B C7–(H)···O2′ contacts; PyrNN is in polychrome, C_6F_6 in green. Both views look straight down the Scheme 4 N–O2···(H)–C4′ rail contacts that parallel the *b*-axis. The *b*-axis goes into the page in both views.§

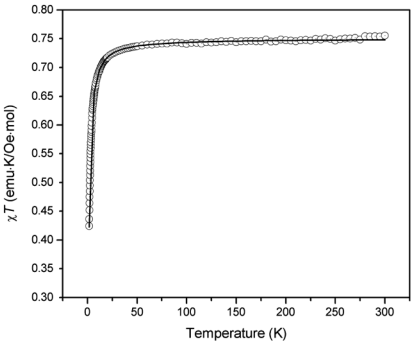

Fig. 15 Magnetic χT *vs.* T data for $(PyrNN)_2 \cdot C_6F_6$ in dc external field of 1000 Oe; solid line shows fit to a 1-D Heisenberg AFM model as described in the text.

means a *low* spin computed ground state. The energy gaps are so small that quite minor changes in crystallographic geometry at low temperature might change even the sign of the estimated interaction. But, the computations show that some exchange can take place through close contacts from the N–O groups to the small spin densities on the nitronylnitroxide methyl groups, not just through close contacts between the large spin density N–O groups. Other experimental work supports this.[2e]

Conclusions

Pyrene functionalized with nitronylnitroxide and iminoylnitroxide gives crystal lattices that are dominated by pyrene CH–π interactions, and by NO···ON and NO···HC contacts. The two polymorphs of PyrNN that were studied – including a newly discovered one – both featured NO···ON contacts.

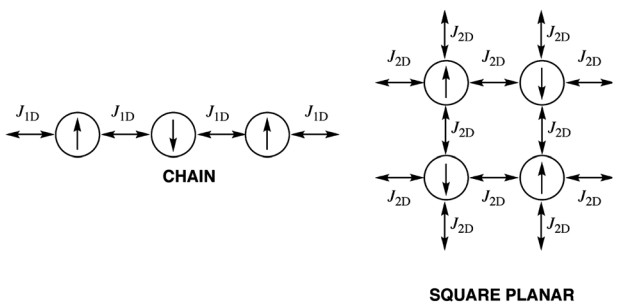

Scheme 5 Intermolecular exchange schemes tested for the $(PyrNN)_2 \cdot C_6F_6$ co-crystal phase.

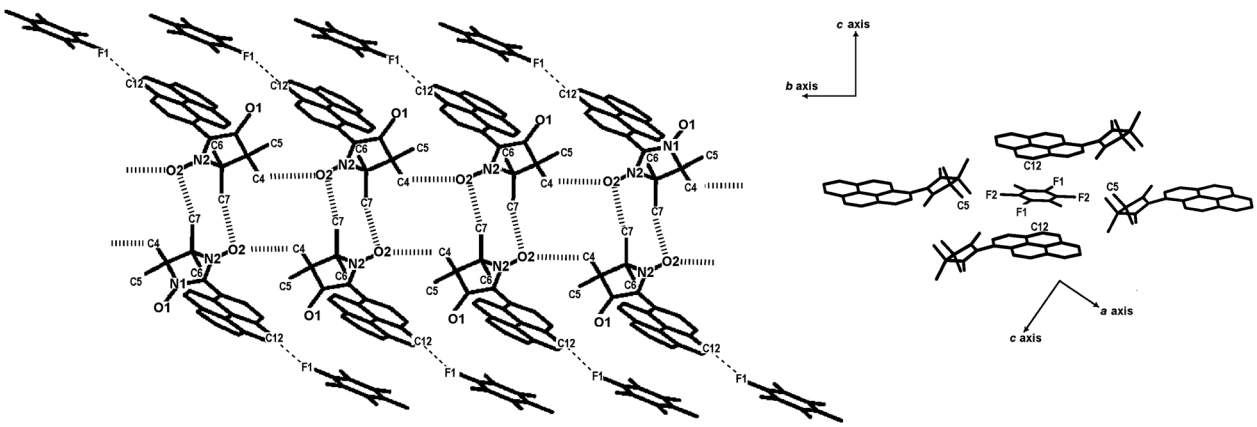

Scheme 4 Interchain rung B (C7·O2′) and rail contacts (C4···O2′) formed in the $(PyrNN)_2 \cdot C_6F_6$ co-crystal (left); interchain PyrNN to C_6F_6 contacts. Hydrogen atoms are omitted for ease of viewing. The (C6·O1′) rung A contacts are not shown here (see Fig. 14).

The previously known α-polymorph has only half of its molecules related by NO···ON contacts; we found it to be magnetically only half spin-paired. The new PyrNN polymorph is fully spin paired because all of its molecules have close NO···ON contacts. A new polymorph was also discovered for PyrIN. The previously reported PyrIN form exhibits strongly spin paired magnetic behaviour due to close NO···ON contacts, while the new polymorph is essentially paramagnetic. The close NO···ON contacts in the α-PyrIN crystal structure were critical to encouraging a new evaluation of the PyrIN magnetism, which in turn led to finding the allotropic β-PyrIN. These findings exemplify the fact that polymorphism is a common complication of soft materials chemistry, for which one must be alert in study of organic molecular magnetic systems. This is especially true given the large effects that modest differences in crystallography can have on magnetic behaviour of organics. For example, the first reported organic ferromagnet, 2-(*p*-nitrophenyl)-4,4,5,5-tetramethyl-4,5-dihydro-*1H*-imidazole-3-oxide-1-oxyl has four reported allotropes, of which one orders ferromagnetically[19] and another antiferromagnetically.[19,20]

Adding hexafluorobenzene to PyrNN "shepherded" the PyrNN molecules into ladder chains based on a π-stack "sandwich" of two PyrNN molecules with a C_6F_6 molecule between their pyrene moieties. The co-crystal lattice has alternating hexafluorobenzene regions and PyrNN regions; primary contacts between the PyrNN molecules involve N–O···H–C(methyl) interactions, with no close NO···ON contacts. The exchange interactions between PyrNN radicals in the co-crystal are weaker than the spin pairing interactions of the PyrNN allotropes. However the exchange in the co-crystal is extended at least to 1-D nature, rather than being confined to dimer-like behaviour as in the PyrNN phases.

Both strong-but-localized, and weak-but-extended magnetic behaviours can thus be realized by manipulation of the crystallization conditions for PyrNN. The same strategy did not work for PyrIN, possibly because it disorders so easily during crystallization or co-crystallization. Still, the use of shepherding co-crystallization for molecules with no strongly directional intermolecular interaction functionality is a promising strategy to give materials having alternating regions of the shepherd molecule and another molecule of main interest, as in the magnetic spin carrier PyrNN. This can even lead[15] to stabilization of systems that decompose as neat solids. Pursuing both polymorphic crystal lattices and co-crystallization strategies allows a wide range of possibilities for making new molecular solid materials with variable electronic properties – such as magnetism –using both new and previously studied molecules.

Acknowledgements

HA and PML thank the National Science Foundation for support of this work by grant CHE 0809791. MAN thanks CAPES and UFRJ (Brazil) for sabbatical leave support. JRF acknowledges the support of the National Science Foundation under grant nos. DMR-0449516 and DMR-1006519. JTM thanks the Chemistry Department of Tulane University for support of the Tulane X-ray Crystallographic Laboratory.

References

1 C. Rovira and J. Veciana, *CrystEngComm*, 2009, **11**, 2017–2212.
2 (*a*) J. J. Novoaand M. Deumal in *Pi-electron magnetism: from molecules to magnetic materials*, J. Veciana and D. Arčon (eds); Spring-Verlag, New York NY (2001), pp 33–60; (*b*) J. Cirujeda, J. Vidal-Gancedo, O. Juergens, F. Mota, J. J. Novoa, C. Rovira and J. Veciana, *J. Am. Chem. Soc.*, 2000, **122**, 11393–11405; (*c*) D. B. Amabilino, J. Cirujeda and J. Veciana, *Philos. Trans. R. Soc. London, Ser. A*, 1999, **357**, 2873–2891; (*d*) M. Deumal, J. Cirujeda, J. Veciana and J. J. Novoa, *Chem.–Eur. J.*, 1999, **5**, 1631–1642; (*e*) H. Heise, F. H. Köhler, F. Mota, J. J. Novoa and J. Veciana, *J. Am. Chem. Soc.*, 1999, **121**, 9659–9667; (*f*) M. Deumal, J. Novoa, M. J. Bearpark, P. Celani, M. Olivucci and M. A. Robb, *J. Phys. Chem. A*, 1998, **102**, 8404–8412; (*g*) J. Veciana, J. Cirujeda, J. J. Novoa and M. Deumal, in *Magnetic Properties of Organic Materials*, P. M. Lahti (ed.); Marcel-Dekker, New York NY (1999), p 573ff.
3 (*a*) J.-M. Lehn, *Supramolecular Chemistry: Concepts and Perspectives*; VCH: Weinheim, Germany (1995); (*b*) C. A. Hunter, K. R. Lawson, J. Perkins and C. J. Urch, *J. Chem. Soc. Perkin Trans.*, 2001, 651–669; (*c*) C. A. Hunter and J. K. M. Sanders, *J. Am. Chem. Soc.*, 1990, **112**, 5525–5534; (*d*) R. Nandy, M. Subramoni, B. Varghese and S. Sankararam, *J. Org. Chem.*, 2007, **72**, 938–944; (*e*) R.-F. Dou, X.-C. Ma, H. L. Yip, K. Y. Wong, W. M. Lau, J.-F. Jia, Q.-K. Xue, W.-S. Yang, H. Ma and A. K.-Y. Jen, *Langmuir*, 2006, **22**, 3049–3056.
4 (*a*) J. D. Dunitz, A. Gavezzotti and W. B. Schweize, *Helv. Chim. Acta*, 2003, **86**, 4073–4092; (*b*) J. C. Collings, P. S. Smith, D. S. Yufit, A. S. Batsanov, J. A. K. Howard and T. B. Marder, *CrystEngComm*, 2004, **6**, 25–28; (*c*) J. C. Collings, K. P. Roscoe, E. G. Robins, A. S. Batsanov, L. M. Stimson, J. A. K. Howard, S. J. Clark and T. B. Marder, *New J. Chem.*, 2002, **26**, 1740–1746; (*d*) J. C. Collings, K. P. Roscoe, R. Ll. Thomas, A. S. Batsanov, L. M. Stimson, J. A. K. Howard and T. B. Marder, *New J. Chem.*, 2001, **25**, 1410–1417; (*e*) J. H. Williams, J. K. Cockcroft and A. N. Fitch, *Angew. Chem., Int. Ed. Engl.*, 1992, **31**, 1655–1657; (*f*) C. R. Patrick and G. S. Prosser, *Nature*, 1960, **187**, 1021.
5 V. Ovcharenko, S. Fokin and P. Rey, *Mol. Cryst. Liq. Cryst. Sci. Technol., Sect. A*, 1999, **334**, 109.
6 C. Mann, R. Gompper and K. Polborn, 2003, CSD Code ENIZIK, CCDC Deposition #226038, private communication.
7 H. Wang, D. Zhang, X. Guo, L. Zhu, Z. Shuai and D. Zhu, *Chem. Commun.*, 2004, 670–671.
8 Y. Wang, H. Wang, Y. Liu, C. Di, Y. Sun, W. Wu, G. Yu, D. Zhang and D. Zhu, *J. Am. Chem. Soc.*, 2006, **128**, 13058–13059.
9 B. Bleaney and K. D. Bowers, *Proc. R. Soc. London, Ser. A*, 1952, **214**, 451–465.
10 M. J. Frisch, *et al. Gaussian 09 Revision B.01*ed.; Gaussian, Inc: Wallingford CT, 2010. See the full citation in ESI.
11 (*a*) C. Lee, W. Yang and R. G. Parr, *Phys. Rev. B*, 1988, **37**, 785–789; (*b*) A. D. Becke, *J. Chem. Phys.*, 1993, **98**, 5648–5652; (*c*) P. J. Stephens, F. J. Devlin, C. F. Chabalowski and M. J. Frisch, *J. Phys. Chem.*, 1994, **98**, 11623–11627.
12 S. J. Grimme, *J. Comput. Chem.*, 2006, **27**, 1787–1799.
13 For drawbacks of this approach, especially spin contamination by higher multiplicity contributions, *cf.*E. R. Davidson, *Int. J. Quantum Chem.*, 1998, **69**, 241–245.
14 For a high spin state having energy E_{HS} and spin-squared expectation value $\langle S^2\rangle_{HS}$, and a low spin state having E_{LS} and spin-squared expectation value $\langle S^2\rangle_{LS}$ the high spin to low spin energy gap $\Delta E_{HS-LS} = (E_{LS} - E_{HS})/\{\langle S^2\rangle_{HS} - \langle S^2\rangle_{LS}\}$(*a*) K. Yamaguchi, H. Fukui and T. Fueno, *Chem. Lett.*, 1986, 625–628; (*b*) K. Yamaguchi, *Chem. Phys. Lett.*, 1988, **149**, 537–542.
15 R. Hicks, M. Lemaire, L. Öhrström, J. Richardson, L. Thompson and X. Zhiqiang, *J. Am. Chem. Soc.*, 2001, **123**, 7154–7159.
16 K. Awaga, T. Sugawara and M. Kinoshita, *J. Chem. Phys.*, 1986, **85**, 2211–2215.
17 D. D. Swank, C. P. Landee and R. D. Willet, *Phys. Rev. B*, 1979, **20**, 2154–2162.

18 G. Baker Jr, H. E. Gilbert, J. Eve and G. S. Rushbrooke, *Phys. Rev. Lett.*, 1967, **25A**, 207.
19 M. Tamura, Y. Nakazawa, D. Shiomi, K. Nozawa, Y. Hosokoshi, M. Ishikawa, M. Takahashi and M. Kinoshita, *Chem. Phys. Lett.*, 1991, **186**, 401–404.
20 (*a*) Y. Nakazawa, M. Tamura, N. Shirakawa, D. Shiomi, M. Takahashi, M. Kinoshita and M. Ishikawa, *Phys. Rev. B: Condens. Matter*, 1992, **46**, 8906–8914; (*b*) T. Kambe, K. Kajiyoshi, K. Oshima, M. Tamura and M. Kinoshita, *Synth. Met.*, 2005, **154**, 301–304.
21 C. F. Macrae, I. J. Bruno, J. A. Chisholm, P. R. Edgington, P. McCabe, E. Pidcock, L. Rodriguez-Monge, R. Taylor, J. van de Streek and P. A. Wood, *J. Appl. Crystallogr.*, 2008, **41**, 466–470.
22 (*a*) C. P. Landee, A. Delcheva, C. Galeriu, G. Pena, M. M. Turnbull and R. D. Willett, *Polyhedron*, 2003, **22**, 2325–2329; (*b*) D. C. Johnston, M. Troyer, S. Miyahara, D. Lidsky, K. Ueda, M. Azuma, Z. Hiroi, M. Takano, M. Isobe, Y. Ueda, M. A. Korotin, V. I. Anisimov, A. V. Mahajan and L. L. Miller, *arXiv:cond-mat/0001147*, 2000.